DIAGNOSTYKA, 2023, Vol. 24, No. 3

e-ISSN 2449-5220
DOI: 10.29354/diag/172535

INFLUENCE OF THE DISTURBANCE CREATED IN THE MEASURING CHANNEL ON THE READINGS OF THE HOT-WIRE ANEMOMETRIC SENSOR

Szymon NITKIEWICZ [1, 2 *], Ahmed AL-JUMAILY [3]

[1] Department of Mechatronics, Faculty of Technical Sciences, University of Warmia and Mazury, 11 Oczapowskiego St., 10-710 Olsztyn, Poland,
[2] Department of Neurosurgery, School of Medicine, Collegium Medicum, University of Warmia and Mazury, 30 Warszawska St., 10-082 Olsztyn, Poland,
[3] Institute of Biomedical Technologies, Auckland University of Technology, WZ Building Level 9, 6 St Paul St, Auckland 1010, New Zealand
[*] Corresponding author, e-mail: szymon.nitkiewicz@uwm.edu.pl

Abstract

The research presents issues related to fluid mechanics, thermodynamics, and statistics. In the first sections, the authors review methods and parameters of fluid measurements. The work mainly emphasizes measurements concerning the parameters of air flows during human breathing. In the following section, the test bench for the analysis is described, and the methodology of data acquisition is described. Finally, the authors present a numerical model of the measurement channel and its calculations compared to measurements from an actual test stand. The data acquirement was performed with LabVIEW, modeling with COMSOL Multiphysics®, and calculations with MATLAB software.

Keywords: flow, numerical modeling, fluid mechanics

List of Symbols/Acronyms

Δd – displacement [m],
t – time [s],
V – speed [m/s],
r/R – relative radius
D – diameter of the pipeline [mm],
d – diameter of the flow hole in the measuring orifice [mm],
l_1, l_2 – distances of the differential pressure collection points from the measuring orifice [mm],
DE – disruptive element,
DC – direct current (motor),
CTA – constant temperature thermos-anemometer,
CCA – constant current thermos-anemometer,
q_v – stream velocity,
U – voltage,
A, B, n – constants (parameters)

1. INTRODUCTION

Accurate airflow measurement is essential in various fields, including aerodynamics, ventilation systems, and biomedical research. Numerous methods have been developed to quantify airflow, each with its strengths and limitations. The authors will quote a few in this paper to indicate their properties.

In fluid mechanics, the environment we conduct our measurements can be classified as a closed or an open conduit. It is of utmost significance to determine the fluid flow configuration, which can either naturally exist or be intentionally manipulated to aid in the measurement process. A pipeline with a predetermined cross-sectional shape, such as a circular one, falls under the category of a closed conduit. However, any conduit with an unspecified cross-sectional shape is classified as an open conduit.

Flowmeters can be divided according to the following classification [1] :

(i) instruments using hydrodynamic methods:
- with variable pressure drop,
- with a variable level,
- with a constant pressure drop,
- vortex,

(ii) instruments with a constantly moving element:
- tachometric,
- Coriolis force,
- with a vibrating element,

(iii) instruments using physical phenomena:
- thermal,
- acoustic,
- optical,
- ionization,
- isotopic,
- Doppler effect,
- measurements using coherent radiation,

Received 2023-07-20; Accepted 2023-09-19; Available online 2023-09-20

iv) instruments using other methods:
- correlation,
- concentration,
- etc.

Some of the sensor types listed are suitable for measuring a wide range of fluids while using others has significant limitations. Selected types of flowmeters will be described below [1]–[4].

Instrumentation for flow measurement can also be categorized on the degree of invasiveness associated with the measurement technique. Because of such a division, we have non-invasive devices and those that affect the measured medium. According to this, we can divide them as follows:

(i) Invasive devices:
- orifices,
- rotameters,
- turbine anemometers,
- calorimeters,
- etc.

(ii) non-invasive devices:
- ultrasound anemometers,
- laser anemometers,
- methods based on the Doppler effect,
- interference of light beams,
- etc.

1.1. Common devices and methods of flow measurements

Airflow analysis has several characteristic parameters, e.g.: - velocity, gradient: temperature, density, pressure, humidity, and volume. Each of the parameters mentioned above requires the use of different measurement techniques.

Basic research in technological applications often deals with the measurement of flow velocity. At the same time, it is a complex metrological issue, especially relating to slow flows. This fundamental parameter is defined as the change in position over time. Referring to the basic speed formula, it is calculated as follows:

$$V = \frac{\Delta d}{t} \tag{1}$$

Where:
V – speed,
Δd – displacement,
t – time.

At this point, the authors would like to recall some of the most common measurement methods.

The most common types of flowmeter are flowmeters with variable pressure drop-measuring orifices. Known for years and successfully used, orifice flowmeters come in many varieties. Local narrowing of the pipeline causes a change in the potential energy of the fluid's static pressure, which is the primary measurement principle in this type of flowmeter. The narrowing in the flow channel causes a pressure drop and, thus, an increase in fluid velocity.

Figure 1 shows one of the classic types of measuring orifices; the simplest construction of this type of flow meter is the orifice. The point of receiving the differential pressure Δp additionally classifies the type of instrument [4], [5]:

Orifices are distinguished by the reception points as follows:
- parathyroid, i.e., $l_1 = l_2 \approx 0$,
- vena contracta, i.e., $l_1 = (0{,}5 \div 2)D;\ l_2 = (0{,}2 \div 0{,}8)D$,
- radial, i.e., $l_1 = D;\ l_2 = 0{,}5\ D$
- flanged, i.e. $l_1 = l_2 \approx 2{,}54\ mm$ or $l_1 \approx l_2 = \frac{D}{2}$

In Fig. 1 two types of measuring orifice are shown, with radial and (a) and radial (b) flanged.

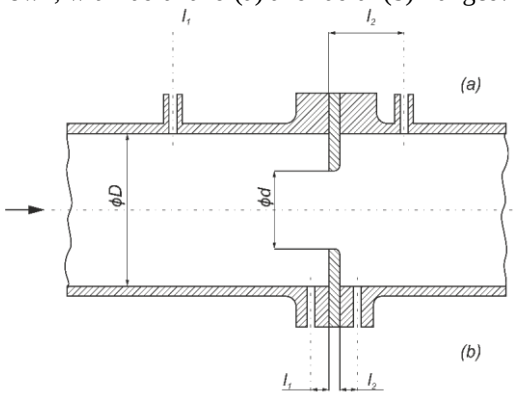

Fig. 1. Measuring orifice types (a) and (b) [4], [5]

where:
D - diameter of the pipeline *[mm]*,
d – diameter of the flow hole in the measuring orifice *[mm]*,
l_1, l_2 – distances of the differential pressure collection points from the measuring orifice *[mm]*.

The main advantages of measuring orifices are their simple design and their simple and easy operation. The popularity of the use of orifices makes it easy to predict their behaviour under various operating conditions, and their performance characteristics are well known. Fig. 2 shows a typical fluid flow through the orifice, with the pressures marked at the measurement points.

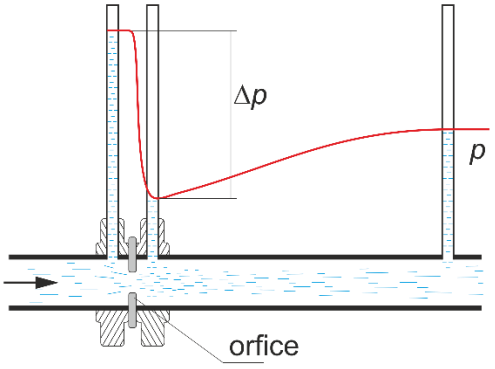

Fig. 2. The change in the pressure (p) of the fluid as it flows through the orifice [4], [5]

The use of thermal pulse flow time is also one of the methods to determine the velocity of the flowing fluid. The determination of the transit time of the thermal pulse is used to extract flow rate

information. At least one heating element (H) and one additional thermal sensor (T) are required. A short thermal pulse is sent from the heater to the surrounding fluid. The heating element should be thermally insulated from the environment/duct to eliminate interference from heat conduction effects. The thermal sensor detects the heat pulse initiated by the heater, as shown in Fig. 3 [6], [7].

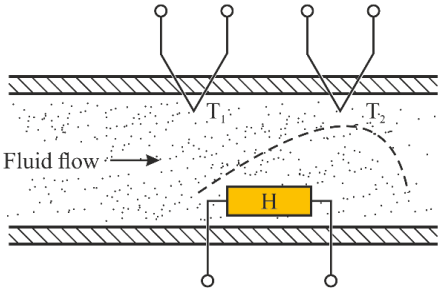

Fig. 3. Diagram of the principle of the calorimetric flowmeter with the course of the temperature of the flowing fluid (dashed line) [6], [7]

Another example of a temperature-based sensor is a hot-wire anemometer. The principle of operation of hot-wire anemometers is using heat loss through the heated element (surface). Heat loss occurs when a heated element is washed with a medium with a lower temperature. As the temperature of the heated element changes, its resistance changes. Currently, in the construction of thermoanemometers, we distinguish two basic systems. The first is the constant-temperature thermoanemometer (T_w = Const., CTA), where the filament's temperature is kept constant, regardless of the speed of the flowing fluid. The second system is a constant-current anemometer (I_w = Const., CCA), whose operating principle consists of maintaining a constant current intensity, unchanging during the measurement of the flow of the medium. Schematic diagrams of bridge systems for both types of hot-wire anemometers are shown in Figures 4 and 5. During fluid flow, contact with the heating element causes heat dissipation [6]–[10].

In addition to the two leading systems mentioned above, there are other solutions for the measuring sensor, for example, supplying the sensor with constant power and voltage; there are also pulsed systems for supplying the thermoanemometric sensor [11], [12].

In the CCA configuration, there is a risk of burning the wire/filament if the cooling airflow is insufficient. Similarly, if the flow is too high, the wire needs to heat up enough to provide measurements with satisfactory accuracy. For these reasons, most hot-wire anemometers are made in a constant-temperature configuration [3], [9], [10], [13]. Properly selected fiber material changes its resistance under the influence of temperature. The intended application of the sensor determines the use of the appropriate sensing element material. Typical materials from which the hot-wire anemometer is made are aluminum, copper, gold, iron, nickel, palladium, platinum, silver, and tungsten.

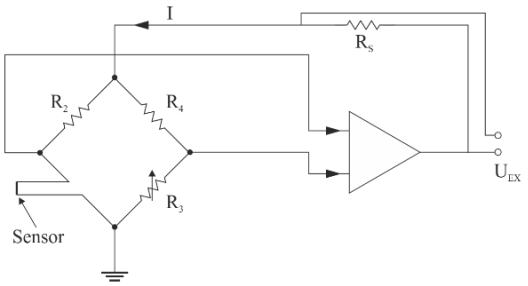

Fig. 4. Scheme of the anemometer in CTA configuration [9]

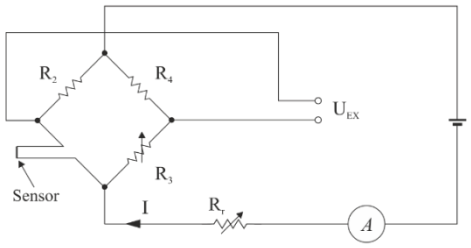

Fig. 5. Scheme of the anemometer in CCA configuration [9]

Appropriate positioning of the sensor fibers makes measuring the fluid stream's speed and direction possible. The authors focus on measuring one velocity component in the presented work, hence choosing a single-fiber sensor, as in Fig. 6 (a). Orthogonal to the direction of the flowing fluid, the position of the anemometer fiber allows the measurement of successive components of the direction, fluid flow velocity, Fig. 6 (b, c) [14], [15].

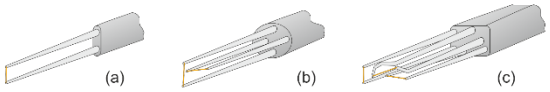

Fig. 6. Examples of hot-wire anemometer probes (a) single-fiber, (b) two-fiber, (c) three-fiber [14], [15]

Another advantage of thermoanemometric sensors is the possibility of sampling the signal with a frequency of up to about 100 kHz at the speed of the flowing medium of about 30 m/s for a measuring element (fiber) with a diameter of 5 μm [10], [16], [17].

Velocity measurements using the method mentioned above are carried out using a fiber placed on supports and connected to an electronic system intended to power the system and is the source of the measurement signal. In such a solution, a conditioning system is necessary to convert the electrical value associated with the voltage drop on the heated fiber to an approximate measured value.

According to King's equation (2), determining the parameters of the processing function allows using a relationship in the measurements to estimate

the instantaneous values of the velocity of the flowing medium q_v, the instantaneous values of the transducer's voltage signal.

$$q_v = [(U^2 - A)B]^n \quad (2)$$

where *A, B, n* are obtained by minimization of equation (3), and *U* is the voltage signal of the thermoanemometric transducer.

$$\left[[(U^2 - A)B]^n - q_{v_r}\right]^2 = min \quad (3)$$

where q_{v_r} is the flow rate value generated by the reference system.

Various measurement methods can be used to determine the flow velocity. One of them is the "Log-Chebyshev" method. The starting point for determining the flow velocity using this method is the hypothesis that the mathematical form of the law of velocity distribution depending on the distance from the wall in ducts on the perimeter of the cross-section is a logarithmic function, and in other elements - a polynomial function.

In this method, the weighting factors were assumed to be equal, so the flow velocity is equal to the arithmetic mean of the local velocities measured at the designated points.

For a circular cross-section, the locations of the measurement points correspond to the values of the relative radius *r/R* shown in Table 1. A single measuring point can be used for a small diameter of the duct.

Table 1. Location of measurement points for a circular cross-section

Number of measuring points on the radius	*r/R*
3	0.375 0.925 0.936
4	0.331 0.612 0.800 0.952
5	0.287 0.570 0.689 0.847 0.962

Figure 7 shows the location of the measurement points in a round duct for the "Log-Chebyshev" method [18]–[20].

For a duct with a rectangular cross-section, a different arrangement of measurement points is assumed; however, in this article, the authors focused on a duct with a round cross-section. Hence only this description has been quoted.

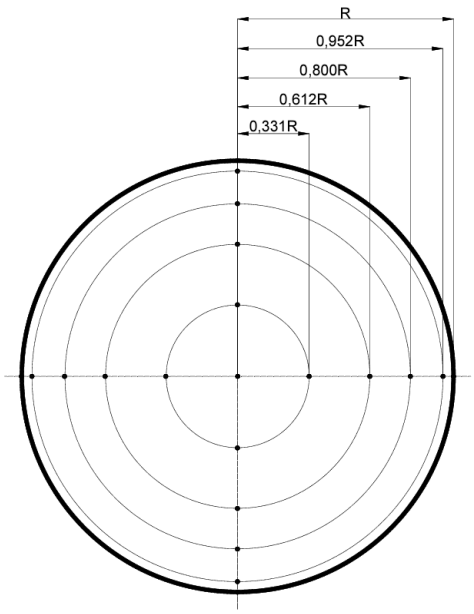

Fig. 7. Location of measurement points in a round duct in the "Log-Chebyshev" method [18]–[20]

1.2. Aim of the work

The aim of the article is to examine the relationship between the position of the disruptive element (DE) on the reading from the air flow sensor. This is related to supporting the diagnosis of the upper respiratory tract [21]–[23]. The shape of the nostrils determines the profile of the air stream exhaled. The appropriate location of the measuring element in the sensor enables the measurement of human breathing parameters with sufficient accuracy [22], [24], [25].

2. METHODOLOGY

As a measuring device, the authors have chosen the CTA due to its metrological properties [13], [21]–[23], [26]. The manufacturer, Strata Mechanics Research Institute, Polish Academy of Sciences, Cracow, Poland, calibrated the sensors.

As a result of the calibration, determined employing the calibration stand, the dependency between the output voltage of the thermoanemometric system *U* connected to the appropriate measuring probe and the flow volume stream q_v was obtained. Examples of measured values used for calibration are shown in Table 2 and Fig. 8 (blue dots) [27].

As a result of the optimization procedures, the coefficients of the processing function (2) with the values presented below were obtained:

$$q_v = [(U^2 - 14.132)0.034]^{2.242} \quad (4)$$

According to Equation 4, the sensor calibration result is shown in Figure 8 (red line) [27].

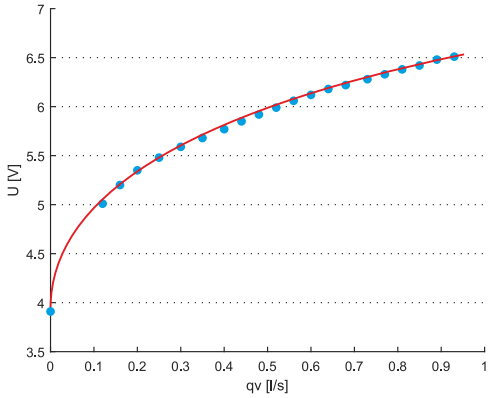

Fig. 8. Calibration results where on the X-axis is qv [l/s], on the Y-axis U [V]

Table 2. Measured results

Probe 1	
q_v *[l/s]*	*U [V]*
0.00	3.91
0.12	5.01
0.16	5.20
0.20	5.35
0.25	5.48
0.30	5.59
0.35	5.68
0.40	5.77
0.44	5.85
0.48	5.92
0.52	5.99
0.56	6.06
0.60	6.12
0.64	6.18
0.68	6.22
0.73	6.28
0.77	6.33
0.81	6.38
0.85	6.42
0.89	6.48
0.93	6.51

2.1. Test stand and sample measurements

A dedicated measuring station was constructed to assess the influence caused by the disturbance introduced into the measuring channel with a different flow velocity, incorporating the ability to modify the disruptive element (DE) that affects the fluid flow. The schematic diagram of a test stand is presented in Fig. 9. The sensor used during the tests was a constant-temperature hot-wire anemometer (CTA) placed at the end of the measuring duct.

The tests were carried out at four different airflow velocities caused by the varying supply voltage value of the DC motor driving the fan. In order to maintain the repeatability of the motor supply voltage, voltage stabilizers of 3V, 5V, 9V, and 12V were used. Experiments were performed with and without the flow disturbance element in the measuring duct. The tests were carried out using three different shapes of the flow disturbance element; the cross-section of each of them is as shown in Figure 10.

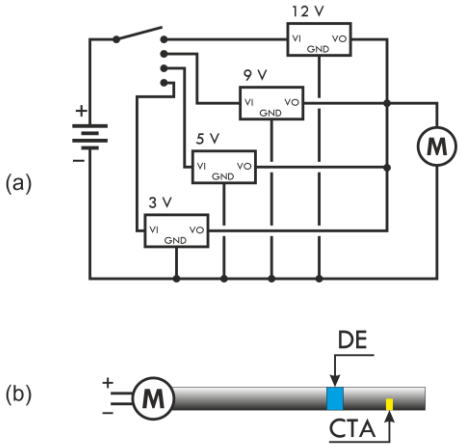

Fig. 9. Test stand with the disruptive modifier (a) power supply scheme, (b) fan with a test duct, disruptive element (DE) and CTA sensor

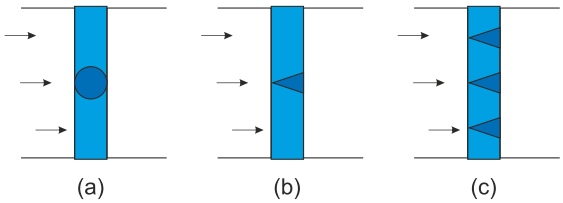

Fig. 10. Cross-sections of the flow disturbance elements applied to the test duct

For clarity, only one case of the flow disturbance element has been described, while the numerical values will be presented in the following.

All measurements were acquired using NI USB-6002 DAQ with 1000 samples/s, LabVIEW software (National Instruments Inc., Austin, TX, USA) with a dedicated programme.

3. RESULTS

The measurements (velocities) were carried out at the beginning of the duct. In Table 3, the authors present the airflow velocities (denoted in the following tables as v_{av}) at the beginning of the duct. These values were needed to provide the numerical model performed using COMSOL Multiphysics® software (COMSOL, Inc., Burlington, MA, USA).

Table 3. Measured velocities at the beginning of the test duct

V_{in}	l/s	m/s
3	0.260	0.684
5	0.489	1.289
9	0.945	2.486
12	1.231	3.236

A simplified model was used for the analysis in the COMSOL Multiphysics® program due to the complexity of the object and MESH computational

problems in the program, which could last from several hours to several days in the case of a change in velocity at the inlet of the measuring channel.

The model considers two cases: a duct without the flow disturbance element and a duct with the circular flow disturbance element. In Figures 11 and 12, modeling sample data from the COMSOL program have been shown. The speed of airflow in the designated measurement sections in the measurement channel and its performance at the inlet and outlet are presented.

The same investigations were conducted for four fun supply voltages (v_{in} ={3V, 5V, 9V, 12V}). The average value of 5 consecutive measurements (of 180000 samples each) is presented in Table 4.

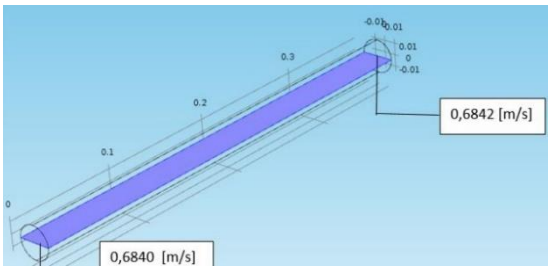

Fig. 11. COMSOL modeling data without disturbance element for 3V supply voltage

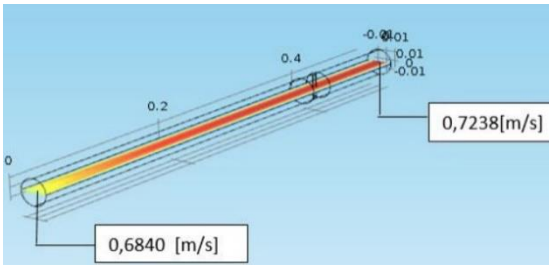

Fig. 12. COMSOL modeling data with circular disturbance element for 3V supply voltage

Table 4. Modelled velocities in the test duct with circular disturbance element

V_{in}	l/s	m/s
3	0.275	0.724
5	0.513	1.438
9	0.980	2.578
12	1.324	3.483

4. DISCUSSION

The modeling data show different values of the velocities in the test duct from the measured one. Table 5 presents the measured and modeled values with and without the disturbance element.

The relationship between modeled and measured values is shown in Table 6.

The velocity values of each of the four cases (no DE, circular, triangle, 3 triangles DEs) are presented in Table 7. As can be observed, the standard deviation (SD) calculated for measurements with and without the disruptive element differ significantly. This could be related to the shape of the airflow after the distortion [28].

Table 5. Measured and modeled velocities *[m/s]* in the test duct with and without a circular disturbance element

	without disturbance		with circular disturbance	
V_{in}	measured	modeled	measured	modeled
3	0.684	0.6842	0.6959	0.7238
5	1.289	1.2891	1.3785	1.4376
9	2.486	2.4864	2.6200	2.7359
12	3.236	3.2363	3.4829	3.5798

Table 6. The ratio of modeled and measured values

V_{in}	without disturbance ratio mod./meas.	with circular disturbance ratio mod./meas.
3	1.0003	1.0401
5	1.0001	1.0428
9	1.0002	1.0442
12	1.0001	1.0237

Table 7. The ratio of modeled and measured values

V_{in}	type of disturbance	v_{av} [m/s]	SD v_{av} [m/s]
3	no distr.	0.684	0.018
5		1.289	0.019
9		2.486	0.044
12		3.236	0.055
3	circular	0.724	0.002
5		1.438	0.008
9		2.578	0.017
12		3.483	0.020
3	triangle	0.751	0.002
5		1.441	0.007
9		2.611	0.014
12		3.510	0.019
3	3 triangles	0.755	0.003
5		1.421	0.008
9		2.582	0.016
12		3.499	0.019

The simulation results differ slightly in comparison with the values determined from the measurements. However, the growth mechanism in the velocity value has been preserved, confirming that the model's study and simulation illustrate this process well. The differences in the results may be dictated by calculation errors in the program or by too large MESH, which was reduced due to the duration of too-long simulation analyses.

Placing a disruptive element on the airflow in the measurement channel leads to an increase in the flow velocity in the vicinity of it, compared to the velocity of the inlet air.

In the study the flow sensors were that have been employed that had been previously subjected to comprehensive testing to assess their repeatability of measurement and measurement accuracy. These assessments are fundamental components of characterizing Type A Uncertainty [29]. In each of

the test measurements carried out, over 98% of the measured values were within the range of the mean value ±3 standard deviations.

Measurements taken at lower voltages, i.e., at lower air velocity and volume at the inlet, show that the measurements are more concentrated than those of higher velocities.

The tests described in this article are used to assess the appropriateness of the sensors' placement during airflow tests in patients with respiratory disorders [21], [22]. This type of examination is used to support the diagnosis of upper respiratory tract pathologies in patients with respiratory disorders [24], [25].

The simulation, model, and conducted tests confirm the hypothesis of turbulent flow induced by the nostrils and the nasal septum. Examination of the airflow in the measuring channel disturbed by an obstacle may suggest the need to move the sensor away from the mouth of the nostrils.

ACKNOWLEDGMENTS

The publication was written as a result of the author's internship at the Institute of Biomedical Technologies, Auckland University of Technology, Auckland, New Zealand, co-financed by the European Union under the European Social Fund (Operational Program Knowledge Education Development), carried out in the project Development Program at the University of Warmia and Mazury in Olsztyn (POWR.03.05. 00-00-Z310/17).

Author contributions: *research concept and design, S.N., A.A.-J.; Collection and assembly of data, S.N.; Data analysis and interpretation, S.N.; Writing the article, S.N., A.A.-J.; Critical revision of the article, A.A.-J.; Final approval of the article, S.N, A.A.-J.*

Declaration of competing interest: *The authors declare that they have no known competing financial interests or personal relationships that could have appeared to influence the work reported in this paper.*

REFERENCES

1. Kabza Z, Kostyrko K. Metrologia przepływów, gęstości i lepkości, 1st ed. Opole: Wyższa Szkoła Inżynierska 1995.
2. Elsner JW, Drobniak S. Metrology of turbulent flows, (pol. Metrologia turbulencji przepływów). in flow machines (pol. Maszyny przepływowe). Zakład Narodowy im. Ossolińskich. 1995.
3. Sydenham PH, Thorn R. Handbook of measurement science, volume 2: practical fundamentals. in Handbook of Measurement Science. Wiley 1991.
4. LaNasa PJ, Loy Upp E. Fluid flow measurement, a practical guide to accurate flow measurement, 2nd ed. Oxford: Elsevier. 2002.
5. Esposito S. Fluid mechanics: a short course for physicists, by Gregory Falkovich. Cambridge University Press. 2012; 53(3). https://doi.org/10.1080/00107514.2012.661779.
6. Frenzel TMF, Grothey H, Habersetzer C, Hiatt M, Hogrefe W. Industrial flow measurement basics and practice. ABB Automation Products GmbH. 2011.
7. Kuo JTW, Yu L, Meng E, Micromachined thermal flow sensors–A review. Micromachines. 2012; 3: 550–573. https://doi.org/10.3390/mi3030550.
8. OA Technical Reference Seriece, Flow & level measurements. OMEGA's Transactions in Measurement & Control 2001. Putman Publishing Company and OMEGA Press LLC. 2001; 4.
9. Perry AE, Morrison GL. A study of the constant-temperature hot-wire anemometer. Journal of Fluid Mechanics. 1971; 47(3): 577–599. https://doi.org/10.1017/S0022112071001241.
10. Eguti CCA, Vieira EDR. Development of a basic circuit of a hot-wire anemometer. 10 Brazilian Congress of Thermal Sciences and Engineering. 2004; 1: 2–6.
11. Sarma GR. Transfer function analysis of the constant voltage anemometer. Review of Scientific Instruments. 1998; 69(6): 2385–2391. https://doi.org/10.1063/1.1148964.
12. Foss JF, Bohl DG, Hicks TJ. The pulse width modulated - constant temperature anemometer. Measurement Science and Technology. 1996; 7(10): 1388. https://doi.org/10.1088/0957-0233/7/10/009.
13. Jamróz P, Ligęza P, Socha K. Dynamic properties of hot-wire anemometric measurement circuits in the aspect of measurements in mine conditions. Archives of Mining Sciences. 2012; 57(3): 699–714. https://doi.org/10.2478/v10267-012-0045-y.
14. Buchczik D, Ilewicz W, Piotrowski J, Waluś S, Wyżgolik R, Żelazik J. Pomiary: czujniki i metody pomiarowe wybranych wielkości fizycznych i składu chemicznego. Warszawa: Wydawnictwa Naukowo-Techniczne. 2015.
15. Jørgensen FE, Dantec Dynamics. How to measure turbulence with hot-wire anemometers: a practical guide. Dantec Dynamics 2005.
16. Hutchins N, Monty JP, Hultmark M, Smits AJ. A direct measure of the frequency response of hot-wire anemometers: temporal resolution issues in wall-bounded turbulence. Experiments in Fluids. 2015; 56 (1):1-4. https://doi.org/10.1007/s00348-014-1856-8.
17. Watmuff JH. An investigation of the constant-temperature hot-wire anemometer. Experimental Thermal and Fluid Science 1995; 11(2): 117–134. https://doi.org/10.1016/0894-1777(94)00137-W.
18. Polish Norm PN–ISO 5221:1994. Rozprowadzanie i rozdział powietrza - Metody pomiaru przepływu strumienia powietrza w przewodzie.
19. Kowalczyk MJ, Łęcki M, Romaniak A, Warwas B, Gutkowski G. Investigations of thermal-flow characteristics of minichannel evaporator of air heat pump. Archives of Thermodynamics. 2021; 42(4): 261–279. https://doi.org/10.24425/ather.2021.139662.
20. American Society of Heating, Standard Methods For Air Velocity And Airflow Measurement. ANSI/ASHRAE Standard 41.2-2018.
21. Kukwa A, Zając A, Barański R, Nitkiewicz S. Zestaw do monitorowania drożności dróg oddechowych. Patent, 2016;P.419511.
22. Nitkiewicz S, Barański R, Kukwa A, Zając A. Respiratory disorders – measuring method and equipment. Metrology and Measurement Systems. 2018; 25(1): 187–202. https://doi.org/10.24425/118157.
23. Kukwa A, Zając A, Barański R, Nitkiewicz S, Zakrzewska M. Anatomical and functional evaluation of the upper airway patency - a multidisciplinary

cooperation. Pulmonary and cardiological clinical cases. Pracownia Wydawnicza Elset. 2018; 81–92.
24. Kukwa A, Zając A, Barański R, Nitkiewicz S, Kukwa W, Zomkowska E, Rybak A. Anatomical and functional assessment of patency of the upper respiratory tract in selected respiratory disorders – Part 1. Metrology and Measurement Systems. 2021; 28(4): 813–836. https://doi.org/10.24425/mms.2021.138538.
25. Zając A, Kukwa A, Barański R, Nitkiewicz S, Zomkowska E, Rybak A. Anatomical and functional assessment of patency of the upper respiratory tract in selected respiratory disorders – part 2. Metrology and Measurement Systems. 2022; 29(3): 429–454. https://doi.org/10.24425/mms.2022.142273.
26. Ligęza P. Rozprawy, monografie: Układy termoanemometryczne - struktura, modelowanie, przyrządy i systemy pomiarowe. Uczelniane wydawnictwa naukowo-dydaktyczne. AGH. 2001.
27. Jamróz P. Sprawozdanie z wzorcowania sond termoanemometrycznych współpracujących z systemem monitorowania oddechu. Kraków 2018.
28. Vogiatzis II, Denizopoulou AC, Ntinas GK, Fragos VP, Simulation analysis of air flow and turbulence statistics in a rib grit roughened duct. The Scientific World Journal. 2014; 2014: 1–10. https://doi.org/10.1155/2014/791513.
29. Nitkiewicz S, Barański R, Galewski M, Zajączkiewicz H, Kukwa A. Requirements for supporting diagnostic equipment of respiration process in humans. Sensors. 2021; 21(10): 3479. https://doi.org/10.3390/s21103479.

DSc. PhD. Szymon NITKIEWICZ, Assistant Professor in the Department of Mechatronics, Specialist in the School of Medicine, Collegium Medicum, University of Warmia and Mazury in Olsztyn. His work focuses on rehabilitation, biomechanics, and diagnostics devices.

Ahmed AL-JUMAILY is a Professor of Biomechanical Engineering at the Institute of Biomedical Technologies, School of Engineering, Computer and Mathematical Sciences, Auckland University of Technology, Auckland, New Zealand. He is the founder and former Director of AUT's IBTec. Al-Jumaily's current research focuses on biomedical applications, with particular interest in the applications of vibration and acoustics to airway constriction therapies and artery non-invasive diagnostics.